Southern Hemispheric Annular Mode links to free-drifting iceberg abundance and mass in the Weddell Sea

John Helly ∗,Henry A. Ruhl †,Kenneth L. Smith Jr.‡ ,David Long §

∗University of California, San Diego, San Diego Supercomputer Center and Scripps Institution of Oceanography, †National Oceanography Centre, Southampton, University of Southampton, European Way, Southampton SO14 3ZH,‡Monterey Bay Aquarium Research Institute, 7700 Sandholdt Road, Moss Landing, CA 95039, and §Brigham Young University, Provo, UT 84602

Abstract

West Antarctic ice-shelves are losing mass and experiencing breakup events including collapse of the Larsen B ice-shelf in January-March 2002 and the increased calving from the Filchner-Ronne ice-shelf during 1998-2000. We used a combination of ship-board iceberg surveys and analysis of Radarsat1 images to quantify size-specific iceberg density and mass over time in the Weddell Sea from 1996-2007. The data show expected seasonal changes in abundance, as well as a significant negative relationship with annual climate variability of the Southern Hemispheric Annular Mode. The abundance of icebergs appears to be governed, in part, by a sequential breakage process modulated by climate conditions with a resulting negative relationship between abundance and size-class. The analysis supports the hypothesis that iceberg abundance is increasing in the Weddell Sea in response to atmospheric and oceanic warming. A considerable portion of the icebergs found in the Weddell originate in other parts of the Antarctic continent including the Ross, Shackleton, and Amery ice shelves. Because icebergs impart considerable influence on surrounding air and ocean environments their shifting abundance could have important but poorly quantified impacts on ocean biogeochemistry and ecology.

icebergs | climate | Antarctica | carbon cycle | hydrologic cycle

Abbreviations: SAM, WAIS, EAIS, GPS, ASF, SAR, DAAC, NASA

\body

Antarctica and especially the Antarctic Peninsula and its glaciers and ice-shelves are subject to the effects of climate change due to exposure to the warming influences of circumpolar oceanic and atmospheric circulation and southern Pacific Ocean air masses (1). Because of its unique geography, the Antarctic Peninsula is likely a leading indicator of climate change for the Antarctic continent, as well as other parts of the planet (1-3). Free-drifting icebergs transport considerable amounts of mass, freshwater, heat, and entrained dust and glacial debris from the continent to the open ocean (4). But, understanding of the factors controlling their dynamics over time in the Southern Ocean and Weddell Sea has been limited to a few studies linking warming and melting to specific calving events (5-7). It is likely, though, abundances of free-drifting icebergs are influenced by global warming and variation in the nature and extent of the connections between global-scale temperate and Antarctic climate fluctuation.

The Southern Hemisphere Annular Mode (SAM) index measures the zonal sea-level pressure differential between southern hemispheric mid-and high-latitudes (8) . Over a 30-year period from 1980-2009, significant inter-annual negative correlations exist between the SAM and austral summer melting at regional and continental scales in Antarctica (9). Over decadal scales, however, the relationship between annual SAM and air temperature is positive (Figure S1, Supporting Material) with both Antarctic air temperature and SAM showing a secular increase since 1948 ($p < 0.001$) (10) and Figure S2, Supporting Material). There is no apparent phase lag between the annual SAM and continental-scale air temperature (Table S3, Supporting Material).

With warming continuing, the West Antarctic ice-sheet (WAIS) is losing mass more rapidly than the Greenland Ice Sheet. In West Antarctica, including the Antarctic Peninsula, the ice-shelf has recently undergone an estimated net loss of $86 \times 10^{12}$ kg $yr^{--1}$ (11) . The WAIS is also experiencing breakup events of the associated ice-shelf along the eastern coast of the Antarctic Peninsula. Such losses include the collapse of the Larsen B ice-shelf in January-March 2002 and the large calvings of the Filchner-Ronne ice-shelf during 1998-2000 (11). The breakup of the Larsen-B was preceded by high rates of surface-melting (7). An estimate by the United States National Snow and Ice Data Center indicates that the Larsen-B breakup released an estimated $6.5 \times 10^{14}$ kg of ice into the Weddell Sea. This is comparable in volume to 100 years of the mean annual discharge of the Mississippi River (12). Icebergs spawned by these events traverse northward through the Weddell Sea and into the Scotia Sea primarily as small-to-medium (0.005-2 $km^2$) size icebergs. Icebergs have even been tracked from the far side of the content into the Weddell Sea. While relatively small compared to the large calving event mentioned, these icebergs are abundant, widely distributed and have been shown to produce hotspots of biogeochemical enrichment and biomass production as they melt (4).

Although there have been studies of iceberg abundance, transport and natural history in Antarctica (5, 13-15), there has not been a interannual time-series estimate of mass and abundance of icebergs in the Southern Ocean and therefore no long-term study of the relationships between climate and iceberg dynamics. An quantitative time series is necessary to estimate how much of these losses are occurring as icebergs that are transported away from ice-sheet margins and into the open ocean and to evaluate the delivery of freshwater, inorganic nutrients and ice-rafted debris into the wider ecosystem of the Southern Ocean. These effects are important in assessing changes in the marine ecology of that region and consequences for carbon cycling. Here we report the results of a time-series analysis of iceberg mass, abundance (density), and size-frequency distributions in the Weddell Sea over a recent 11-year period. We then postulate an empirical relationship between the SAM and changes in iceberg abundance dynamics.

## Results

From the analysis of the satellite images, we found intra-annual variation in abundance due to seasonal fluctuations in the extent of sea-ice which restricts the movement of icebergs into open water to the north. This is reflected in the low abundance values from images collected in austral winter (5-6 September 2003) versus elevated abundance values from images collected during the austral summer (e.g., 1996, 1997, 2005, 2006 and 2007). A likely typical decline from peak austral summer values can be seen in the results from 1996 (Fig. 2).

Interannual variability in abundance was roughly as strong as seasonal dynamics. The characterization of annual variation is complicated by the irregular collection of images. The size-frequency distributions between all available images reveal interannual variation in density and mass abundance over the 11-year period that spans the period of major ice-shelf breakup events on the Larsen B (2002) and Filchner-Ronne (1998-2000) ice-shelves (Fig. 2). The size-frequency distributions of total abundance over all size classes show both intra and inter-annual variation in abundance.

The total density, total mass, size-specific density distribution and mass distribution of the studied icebergs were correlated to the SAM ($p < 0.05$). Higher values in the SAM correlated to decreasing total iceberg density and mass, as well as shifts in the size-specific density distributions and size-specific mass distributions ($p < 0.05$). Because seasonal variations were great and there was unavoidably uneven sampling between seasons, we conducted the correlation analysis again using only the summer data.

Significant correlations between annual SAM and total density and mass (Fig 3A), as well as size-density and size-mass distribution indices (Fig. 3B) remained. The summer densities and masses ranged by about two orders of magnitude (Fig 3A), as did the seasonal variations over the full dataset. When the SAM was low, such as in summer 2007, iceberg abundances were elevated with decreasing densities in larger size classes (Fig 4A). Conversely during 1998, a higher SAM year, there were fewer icebergs and a less clear relationship between size class and abundance, apart from the fact that the smallest and largest bergs were relatively less common. A similar relationship was found for mass but with a lesser range of variation between the size classes (Fig. 4B and D). A series of correlations between total density, total mass, size-specific density and mass distribution similarity and successively longer-term averages of SAM indicated that those iceberg dynamics are most negatively correlated with a 3-year SAM running mean (Supporting Online Material).

Discussion

Iceberg populations were dominated by the small size-classes (0.005-0.5 $km^2$) (Fig. 3). These size-specific density distributions (Fig. 4A and C) are expected where relatively large icebergs break apart over time into pieces (14) that lead to a succession of smaller icebergs. Iceberg size-specific density and mass distributions are thought to be related to a systematic mechanism of iceberg breakup, modulated by environmental conditions such as those reflected in the SAM.

With the exception of the large (>4km), actively-tracked icebergs, the spatio-temporal origin of the imaged icebergs is uncertain. Many icebergs in the Weddell Sea originate form other areas such as the Ross, Shackelton, and Amery ice shelves. Icebergs also can calve and later become locked in sea-ice for as much as six years or more depending on environmental conditions and circumpolar circulation. However, when icebergs reach the northeastern Weddell Sea they usually begin to deteriorate rapidly under the warming influences of the Antarctic Peninsula region.

Over annual to interannual timescales the SAM is positively correlated with a strengthening of westerly atmospheric flow and a warming by several kelvins in the Antarctic Peninsula and a cooling of the rest of Antarctica (16). On decadal time scales, however, the relationship between the SAM index and air temperature becomes positive for the continent. Thus the observation that annual iceberg abundances in the Weddell

Sea are negatively linked to multi-year SAM values suggests the importance of processes occurring across seasonal to decadal scales. Many icebergs become entrained seasonally in ice during winter and freed in summer with some additional icebergs being calved in summer. On annual timescales the SAM is negatively correlated through linear and non-linear processes to surface melting across the Antarctic Peninsula as well as the Filchner, Dronning, Amery, Wilkes, Ross, and Ellsworth Lands indicating that this is a widely spread phenomenon in coastal areas (9).

Iceberg abundances in the Weddell Sea over annual scales seem to be linked to climate variations with important influences of calving from outside the Antarctic Peninsula region. This is supported by the warming that occurs over most of the continent and Southern Ocean during low annual SAM periods, as indicated by the negative relationship between annual SAM and air temperature for areas other than the Antarctic Peninsula. Tracking data from larger icebergs also confirm that icebergs in the Weddell can originate from the far side of the continent over those timescales. Icebergs can be produced and later become locked in ice sheets for a season or more depending on environmental conditions, a process consistent with the peak in iceberg abundance correlations with a multi-year SAM running mean.

Over decadal scales the relationship between the SAM index and iceberg abundance likely becomes positive. The SAM index had annual negative correlations between continental-scale air temperature from 1996-2007 that were superimposed on a long-term positive increase in both SAM and temperature since 1948. The SAM index in the 10 years prior to the date of the first Radarsat-1 images showed a positive increase. Therefore, our results suggest that there can be a long-term time lag between the forcing reflected by the SAM index and the breakup of icebergs from the Antarctic Peninsula, as well as ice-shelf breakup and calving events from other areas. Another possibility is that, on short time scales during periods of negative SAM, the continental outflow of air may affect the distribution and density of sea-ice with entrained icebergs and affect their release from seasonal pack ice.

The links of annual-interannual SAM to iceberg dynamics over time shown here suggest the contribution of long-term climate forcing from the atmosphere to the cryosphere and hydrosphere as a mass flux of fresh water. New evidence from acoustic signals in ice sheets also suggest that the passing of ocean gravity waves, which can be related to climatic anomalies, may also influence breakup processes (17). Our research indicates that it should be possible to further connect climatic processes to iceberg dynamics and their ultimate influence on physical and biogeochemical fluxes and related effects on the carbon cycle through the marine food web. Changes in marine productivity related to iceberg production and distribution are believed to directly affect carbon fixation by marine plants and animals and ultimately carbon sequestration in the deep sea (4). The ongoing description of these relationships is providing a basis for the estimation of geophysical and biological spheres of influence in the region of the Antarctic Peninsula and the Weddell Sea. This will contribute appreciably to a more complete description of the effects of climate change on the most sensitive part of the Antarctic continent and its effects on the Southern Ocean.

Our results support a hypothesis that the increases in abundance of icebergs is being forced by warming and melting elated to decreased SAM index over interannual scales. However the temporal resolution of our data prohibits a conclusive indication that decadal warming is leading to long-term increases in iceberg density and mass. The positive relationship between the SAM and air temperature over decadal scales nonetheless suggest the possibility that icebergs have been becoming more abundant for decades. The development of a systematically sampled, long-term quantification of iceberg dynamics from radar satellites or similar images will be required to test this possibility.

## Materials and Methods

In December 2005, we performed ship-based measurements of the elevation and perimeter of four free-drifting icebergs in the Weddell Sea to calculate the volume and mass of individual icebergs. This was done by circumnavigating each iceberg to obtain the time-series of ship-position while measuring the iceberg freeboard with a laser rangefinder and inclinometer. The perimeter was corrected for the stand-off distance of the ship to the ice-face using the laser data and on-board navigational radar. We used these measurements to calculate the sub-aerial volume and from this estimate iceberg mass. Abundance and size class data were obtained by processing archival Radarsat-1 satellite images spanning 11 years (1996-2007) (Supplementary Information, Table S3). Additionally, in 2007, we specifically tasked the collection of Radarsat-1 imagery and therefore have a more regular time-series across four austral summer months. The ship-based measurements were then used to calibrate the iceberg abundances to mass by size-class (cf. Supplementary Information).

ACKNOWLEDGMENTS. We thank all the shipboard scientific personnel on the research vessel Laurence M. Gould cruise LMG05-14A for outstanding support, including R. Wilson, K. Reisenbichler, R. Sherlock, J. Ellena, M. Vardaro, K. Osborn, D. Chakos, J. Derry, L. Ekern, J. Kinsey, C. Koehler, and K. Noble. Captain R. Verret, the officers and crew and the Raytheon Polar Services support group of S. Suhr-Sliester, J. Spillane, P. Fitzgibbons, K. Pedigo, J. Dolan, E. Roggenstein, and D. Elsberg provided the experience and skills needed to make this work possible. This research was supported by NSF grants ANT-0529815, ANT-0650034, and OCE-0327294, and by the David and Lucile Packard Foundation. Radarsat-1 images were provided by NASA grant through the Alaska Satellite Facility as a result of an agreement with the Canadian government that, unfortunately, does not extend to Radarsat-2. We wish to thank R. Sanches and the other members of the User Support Office at the ASF for their invaluable help in obtaining and effectively employing these images.

1. Marshall GJ, Orr A, Lipzig NPMv, & King JC (2006) The Impact of a Changing Southern Hemisphere Annular Mode on Antarcic Peninsula Summer Temperatures. Jounal of Climate 19.
2. Steig EJ, et al. (2009) Warming of the Antarctic ice-sheet surface since the 1957 International Geophysical Year. Nature 457(22 January 2009).
3. Zwally HJ, et al. (2005) Mass changes of the Greenland and Antarctic ice sheets and shelves and contributions to sea-level rise. J. Glaciolology 51(175).
4. Smith K, et al. (2007) Free-drifting icebergs: hotspots of chemical and biological enrichment in the Weddell Sea. Science 317.

5. Scambos T, Sergienko O, Sargent A, MacAyeal D, & Fastook J (2005) ICESat profiles of tabular iceberg margins and iceberg breakup at low latitudes. Geophvs. Res. Lett, 32, L23S09.
6. Shepherd A, Wingham D, Payne T, & Skvarca P (2003) Larsen ice shelf has progressively thinned. Science 302:856--859.
7. van den Broeke M (2005) Strong surface melting preceded collapse of Antarctic Peninsula ice shelf. Geophys. Res. Lett. 32, L12815(doi:10.1029/2005GL023247).
8. Gong D & Wang S (1999) Definition of Antarctic Oscillation Index. Geophys. Res. Lett. 26:459-462.
9. Tedesco M & Monaghan AJ (2009) An updated Antarctic melt record through 2009 and its linkages to high-latitude and tropical climate variability. Geophys. Res. Lett 36(L18502, doi:10.1029/2009GL039186).
10. Nan S & Li J (2003) The relationship between summer precipitation in the Yangtze River valley and the previous Southern Hemisphere Annular Mode. Geophys. Res. Letters 30(24)(doi: 10.1029/2003GL018381):2266.
11. Shepherd A & Wingham D (2007) Recent Sea-level Contributions of the Antarctic and Greenland Ice Sheets. Science 315(16 March 2007).
12. Salazar K (2010) Real-time Streamflow and Water Quality (Mississippi River Basin Discharge to the Gulf). (US Geological Service).
13. MacAyeal DR, et al. (2006) Transoceanic wave propagation links iceberg calving margins of Antarctica with storms in tropics and Northern Hemisphere. Geophysical Research Letters 33(L17502).
14. Schodlok MP, Hellmer HH, Rohardt O, & Fahrbach E (2006) Weddell Sea iceberg drift: Five years of observations. Geophvs. Res., ill, C06018, doi:I0.1029/2004JC002661.
15. Weeks WF, Mellor M, Corps of Engineer USA, Cold Regions Research, & Laboratory E (1978) Some elements of iceberg technology, CRREL Report 78-2.).
16. Thompson DWJ & Solomon S (2002) Interpretation of recent Southern Hemisphere climate change. Science 296(doi:10.1126/ science.1069270):895-899.
17. Bromirski P, Sergienko OV, & MacAyeal DR (2010) Transoceanic infragravity waves impacting Antarctic ice shelves. GEOPHYSICAL RESEARCH LETTERS 37(L02502):6.

Fig. 1. Geographic location and extent of each of the 16 Radarsat images, spanning 11 years, used in the analysis. Each image was sub-sampled to include only ocean areas of free-drifting icebergs away from sea ice. Sampling locations in 2005 for icebergs in Table 1 are shown in red lettering.

Fig. 2. Total iceberg density and mass within each Radarsat1 image. Images are arranged in time order, but are not equally spaced in time.

Fig. 3. Annual SAM plotted versus A) summer total density (•) and mass (◦) with the significant log-linear relationships plotted in solid and dotted lines respectively. These include data from 1996, 1997, 1998, 2006 and 2007. Also shown is annual SAM versus B) a non-metric multi-dimensional scaling (MDS) similarity measure of size-density and size-mass distributions from those same times (MDS x-ordinate shown). All linear regressions relationships were tested for significance using an F-test and resulting *p* values are shown.

Fig. 4. Size specific A) density and B) mass distributions for austral summers when the annual SAM values were lower (summer 2007) and higher (summer 1998). Also shown are the percent size-frequency distributions for the C) density and D) mass data.

| Iceber dynamics | Annual SAM | | Multi-year SAM running means | | | | | | | | | | | | | | | | | |
|---|---|---|---|---|---|---|---|---|---|---|---|---|---|---|---|---|---|---|---|---|
| | | | 2-year | | 3-year | | 4-year | | 5-year | | 6-year | | 7-year | | 8-year | | 9-year | | 10-year | |
| | R | *p* | R | *p* | R | *p* | R | *p* | R | *p* | R | *p* | R | *p* | R | *p* | R | *p* | R | *p* |
| Size-specific density distribution similarity index (MDS x-ord.) | -0.97 | 0.005 | -0.89 | 0.045 | -0.99 | 0.001 | -0.90 | 0.040 | -0.70 | 0.191 | -0.97 | 0.008 | -0.71 | 0.183 | -0.48 | 0.414 | -0.29 | 0.638 | -0.30 | 0.624 |
| Size-specific mass distribution similarity index (MDS x-ord.) | -0.92 | 0.027 | -0.90 | 0.035 | -0.98 | 0.003 | -0.93 | 0.023 | -0.70 | 0.192 | -0.98 | 0.003 | -0.85 | 0.068 | -0.64 | 0.244 | -0.45 | 0.446 | -0.50 | 0.394 |
| Total mass (log $10^{12}$ kg $km^{-2}$) | -0.96 | 0.008 | -0.87 | 0.058 | -0.99 | 0.001 | -0.87 | 0.053 | -0.80 | 0.107 | -1.00 | 0.000 | -0.79 | 0.113 | -0.51 | 0.379 | -0.37 | 0.543 | -0.42 | 0.486 |
| Total density (log ind. $km^{-2}$) | -0.98 | 0.004 | -0.90 | 0.040 | -0.99 | 0.001 | -0.90 | 0.035 | -0.71 | 0.180 | -0.97 | 0.007 | -0.71 | 0.180 | -0.47 | 0.422 | -0.28 | 0.649 | -0.30 | 0.626 |

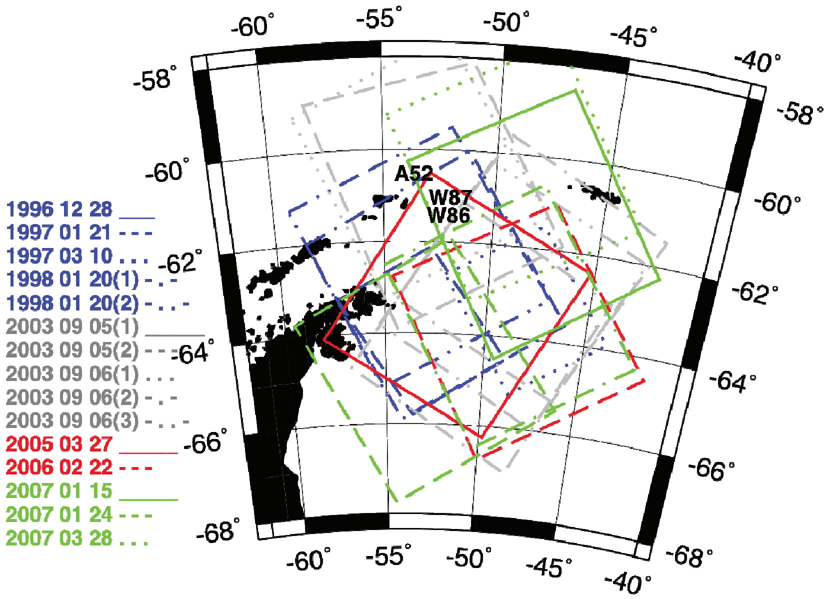

-60°
-55°
-50°
-45°
-40°
-58°
-60°
-62°
-64°
-66°
-68°
A52
W87
W86
1996 12 28
1997 01 21
1997 03 10
1998 01 20(1)
1998 01 20(2)
2003 09 05(1)
2003 09 05(2)
2003 09 06(1)
2003 09 06(2)
2003 09 06(3)
2005 03 27
2006 02 22
2007 01 15
2007 01 24
2007 03 28

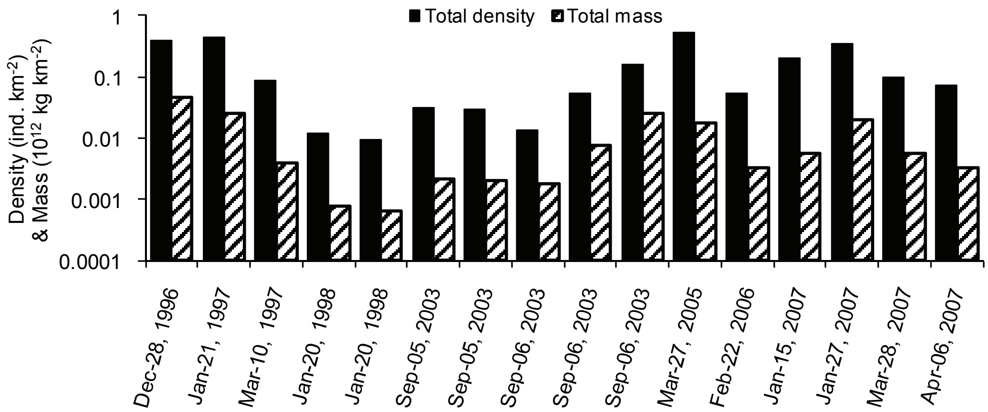

Total density
Total mass
Density (ind. km-2) & Mass (10^12 kg km-2)
1
0.1
0.01
0.001
0.0001
Dec-28, 1996
Jan-21, 1997
Mar-10, 1997
Jan-20, 1998
Jan-20, 1998
Sep-05, 2003
Sep-05, 2003
Sep-06, 2003
Sep-06, 2003
Sep-06, 2003
Mar-27, 2005
Feb-22, 2006
Jan-15, 2007
Jan-27, 2007
Mar-28, 2007
Apr-06, 2007

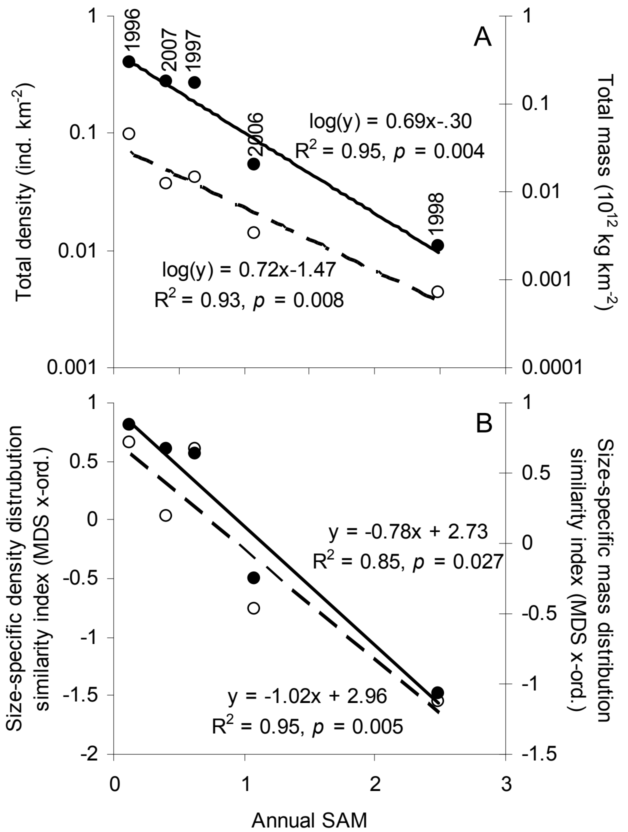

A
B
Total density (ind. km-2)
Total mass (10^12 kg km-2)
1996
2007
1997
2006
1998
log(y) = 0.69x-.30
R2 = 0.95, p = 0.004
log(y) = 0.72x-1.47
R2 = 0.93, p = 0.008
Size-specific density distrubution similarity index (MDS x-ord.)
Size-specific mass distribution similarity index (MDS x-ord.)
y = -0.78x + 2.73
R2 = 0.85, p = 0.027
y = -1.02x + 2.96
R2 = 0.95, p = 0.005
Annual SAM

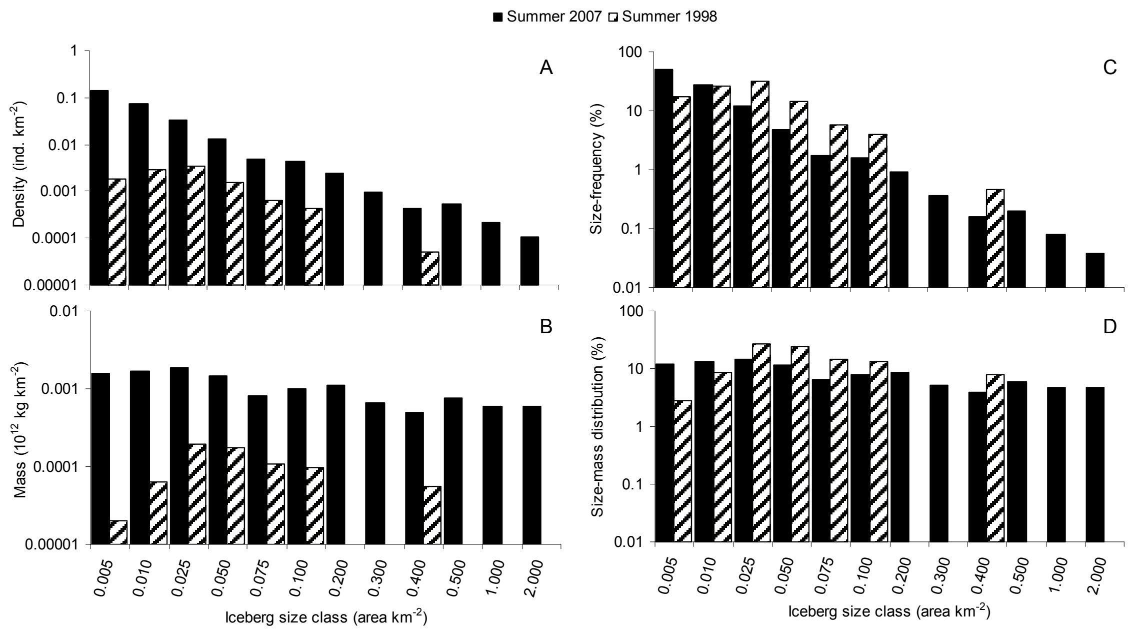
Summer 2007
Summer 1998
A
B
C
D
Density (ind. km-2)
Mass (10^12 kg km-2)
Size-frequency (%)
Size-mass distribution (%)
1
0.1
0.01
0.001
0.0001
0.00001
100
10
0.005
0.010
0.025
0.050
0.075
0.100
0.200
0.300
0.400
0.500
1.000
2.000
Iceberg size class (area km-2)
Iceberg size class (area km-2)

## Materials and Methods

*Iceberg Measurement.*

For each iceberg, we obtained the perimeter by circumnavigating it while making elevation measurements directly abeam the starboard side of the ship using a laser rangefinder and inclinometer (LaserTech Impulse 200XL) mounted on a compass gimbal attached to the bridge railing approximately 80 feet above the waterline. Since the perimeter was obtained from the R/V Laurence M. Gould's GPS navigation data (Ashtech receiver), it was corrected for the standoff distance between the ship and the iceberg as measured by the horizontal range on the bridge navigational radar.

Alternating measurements of horizontal and vertical range and angle, with zero inclination at the point normal to the ice face, were obtained and summed to provide the distance from the top of the iceberg to the waterline (Table S1). These were then averaged to obtain a mean value for the entire perimeter. Exposed area was computed using a triangle decomposition method for arbitrary 2D polygons. A52 was measured at two times separated by 6 days. The first time, A5201, was when it was largest and, A5202, after it had apparently grounded and then regained circulation and begun to break up into numerous pieces.

*Image Processing.*

Level 1 Radarsat-1 SCANSAR/Wideband images were obtained from the NASA Alaska Satellite Facility (ASF) SAR/DAAC using the Earth Observing System Data Gateway with a data grant from NASA (there is no formal citation for this type of grant). These were obtained by searching the satellite image archive for images within the region with the bounding box coordinates [(-55N, -55W), (65S, -42W)] and also by requesting the collection of images in the 2006-2007 austral summer. All resultant images were processed as described below to extract abundance counts of icebergs that were classified by sub-aerial surface area in the range of 0.005-2 km2 into 12 size classes (Table S2).

These are the only images available in this region during the approximate austral summer when there are significant areas free of sea-ice. Of the 16 images, the 12 earliest were discovered in the data archives and the 4 most recent, all collected in 2007, were requested in 2006 specifically for this analysis. As shown in Fig. 1, the images do not all overlap but all do sample the northern region of the Weddell Sea. This is due to the orbital repeat pattern of the satellite, scheduling constraints due to competition for on-board satellite storage resources and terrestrial down-link facilities and to the fact that earliest 12 images were collected for other purposes.

The Level 1 images were processed into GEOTIFFs with a UTM projection using the SARtools software provided by the ASF [1]. An example of the resulting images is presented in Fig. S3, which also depicts a typical subregion within the parent image that was selected for processing. The subregions were then visually inspected to find the maximal rectangular subregion containing icebergs and free of sea-ice, image artifacts and landmass. The subregion was extracted manually using an image cropping tool.

The extracted images were processed in MATLAB by estimating the background, subtracting it from the image, thresholding the result using an image-specific value, conversion of the pixels (50 m x 50 m) to the binary values of black or white and then counting the white objects greater than or equal to two pixels in size (0.005 $km^2$). In

Table S2 the column labeled Area is the area in square kilometers of the sub-image that was processed to derive the counts by size-class for that image. The threshold values are the settings for the contrast level used to discriminate icebergs from background and the disk size is the number of contiguous pixels used to structure the background elements for removal. These vary across images because the illumination, surface texture and reflectance are different in each image and these considerations are important to the removal of background and contrast enhancement before counting icebergs. This process followed the example of counting rice grains presented in the image processing toolbox manual that is part of the MATLAB documentation.

*Iceberg Mass Estimation from Observations.*

Total iceberg mass of Table S1 was calculated as $M_t = V_s$ (850 kg $m^{-3} \times 8$) where the factor 8 is the submerged mass/exposed mass ratio, $M_t$ is the total iceberg mass and $V_s$ is the subaerial volume. The subaerial volume was calculated as described above in the Iceberg Measurement section. The density, 850 kg $m^{-3}$, is estimated from the plot of ice density versus depth in [2] and follows Schodloks usage [3]. The submerged mass/exposed mass ratio accounts for the Archimedes equilibrium ratio, 1 part exposed and 8 parts submerged, of icebergs in water corresponding to the ratio of densities of an iceberg to seawater ($\rho i/\rho s = 8$). The mass of W86 was used to estimate the mass of icebergs less than or equal to 0.3 $km^2$ in area and W87 was used for those greater than 0.3 $km^2$ (Table S1). Mellor and Weeks [4] provide an extensive method of correcting this type of estimate for the presence of submerged terraces which occur on icebergs that tend to ride higher in the water. We have not employed that correction here since our calculation of total iceberg mass is based on the calculation of directly measured exposed mass and not total iceberg volume.

*Climate data.*

The data for the SAM index was obtained from Nan and Li [5] and a copy of the data is provided as downloaded from http://www.lasg.ac.cn/staff/ljp/data-NAM-SAM-NAO/SAM-AAO.htm in February 2010 and used in the analysis here. Mean annual iceberg abundance is plotted along with the SAM index in Figure S2. Air temperature came from the US National Centers for Environmental Prediction and the National Center for Atmospheric Research Reanalysis data (Kistler et al. 2001, Kanamitsu et al. 2002) downloaded from http://www.esrl.noaa.gov/psd/data/gridded/reanalysis/.

*Statistics.*

Statistical analysis and linear regressions were performed with SigmaStat™ software. The multidimensional analysis was performed using Primer-6. The size-specific density and mass distribution similarity was determined by first transforming the distribution data by log(x+1). Then the Brey-Curtis similarity measure was determined between all possible sample pairs and a multi-dimensional scaling (MDS) plot was made using those data. The MDS x-ordinates that appear in Fig. 3B were made using these data.

1. Alaska Satellite Facility Engineering Group. (2006) ASF MapReady User Manual Version 2.2 (University of Alaska, Fairbanks).
2. Swingedouw, D, Fichefet, T, Huybrechts, P, Goosse, H, Driesschaert, E, & Loutre, M. F. (2008) Geophvsical Research Letters 35.

3. Schodlok, M. P, Hellmer, H. H, Rohardt, O, & Fahrbach, E. (2006) Geophvs. Res., ill, C06018, doi:I0.1029/2004JC002661.

4. M. Kanamitsu, W. Ebisuzaki, J. Woollen, S-K Yang, J.J. Hnilo, M. Fiorino, and G. L. Potter. NCEP-DEO AMIP-II Reanalysis (R-2): 1631-1643, Nov 2002, Bul. of the Atmos. Met. Soc.

5. Nan, S., and J. Li, 2003: The relationship between summer precipitation in the Yangtze River valley and the previous Southern Hemisphere Annular Mode. Geophys. Res. Lett., 30(24), 2266, doi: 10.1029/2003GL018381.

6. Kistler, R., E. Kalnay, W. Collins, S. Saha, G. White, J. Woollen, M. Chelliah, W. Ebisuzaki, M. Kanamitsu, V. Kousky, H. van den Dool, R. Jenne, and M. Fiorino, 2001: The NCEP-NCAR 50-Year Reanalysis: Monthly Means CD-ROM and Documentation. Bull. Amer. Meteor. Soc., 82, 247-268.

Fig. S1. Map showing correlation coefficients between the SAM index (denoted as AAO, or Antarctic Oscillation, in this figure) and spatially distributed air temperature at the land/sea surface. The map extends from 58ºS to the South Pole. Temperature data come from the NCEP/NCAR Reanalsis II dataset (Kanamitsu et al. 2002).

Fig. S2. Sixty-year time series illustrating variation in the SAM index and the air temperature for the land/sea surface from 58º to 90ºS as interpolated from the NCEP/NCAR Reanalysis I dataset (Kistler et al. 2001). These time series have a significant positive Pearson correlation ($p < 0.03$) and are both positively correlated to time ($p < 0.001$). When these two series are de-trended, however, they are negatively correlated ($p <0.001$) to each other. Thus, there are different relationships depending on the timescale being considered.

Fig. S3. Radarsat SCANSAR Wide-band image R153785738G3S002 collected on 2006 JD53 (2006 Feb 22) located with center latitude -63.861534, center longitude -54.379646. Antarctic Peninsula and Joinville Islands are in the center with Bransfield Strait to the right. A large iceberg, probably A-22, can be seen in the lower right corner of the yellow rectangle. The sub-sampled area is outlined in yellow illustrating the selection of the image processed for counting icebergs. The constraints require avoidance of sea-ice, land-masses and image artifacts. The particular conditions of the image dictate the values for the threshold and disk size reported in Table S2 used to remove the background and perform contrast enhancement on the residual image before counting icebergs.

Table S1. Measurements of individual icebergs geometry. A52 was measured two times separated by 10 days. The first time, A5201, was when it was largest and, A5202, after it had apparently grounded and then regained circulation and begun to break up into numerous pieces. The elevation measurement is accompanied by standard error.

Table S2. Iceberg abundance sorted by date and size class provided in A) density and B) mass. The image area is the size of the sub-sampled image and the threshold is the contrast threshold used in image processing and disk size is a structuring parameter used to control background removal. Threshold and disk size are both image-specific.

Table S3. Pearson correlations between the listed iceberg dynamics and the Annual SAM, as well as multi-year running means ranging from a 2-year to a 10-year means.

A

| Image metadata | | | | Size-specific density (ind. km$^{-2}$) | | | | | | | | | | | | |
|---|---|---|---|---|---|---|---|---|---|---|---|---|---|---|---|---|
| | | | | Size classes (area in km$^2$) | | | | | | | | | | | | Total |
| Image | Date | Area (km$^2$) | Threshold | 0.005 | 0.01 | 0.025 | 0.05 | 0.075 | 0.1 | 0.2 | 0.3 | 0.4 | 0.5 | 1 | 2 | Density |
| 1 | Dec. 28, 1996 | 9149 | 0.5 | 0.08689 | 0.08897 | 0.07662 | 0.05662 | 0.02842 | 0.03181 | 0.01552 | 0.00568 | 0.00240 | 0.00240 | 0.00044 | 0.00033 | 0.39611 |
| 2 | Jan. 21, 1997 | 14822 | 0.7 | 0.23229 | 0.09297 | 0.04790 | 0.02773 | 0.01680 | 0.01815 | 0.00769 | 0.00223 | 0.00074 | 0.00074 | 0.00027 | 0.00007 | 0.44758 |
| 3 | Mar. 10, 1997 | 28460 | 0.7 | 0.03204 | 0.03018 | 0.01778 | 0.00622 | 0.00186 | 0.00130 | 0.00021 | 0.00004 | 0.00004 | 0.00011 | 0.00007 | 0.00000 | 0.08985 |
| 4 | Jan. 20, 1998 | 20481 | 0.5 | 0.00229 | 0.00347 | 0.00342 | 0.00186 | 0.00073 | 0.00049 | 0.00000 | 0.00000 | 0.00005 | 0.00000 | 0.00000 | 0.00000 | 0.01230 |
| 5 | Jan. 20, 1998 | 19153 | 0.5 | 0.00146 | 0.00219 | 0.00350 | 0.00125 | 0.00052 | 0.00037 | 0.00000 | 0.00000 | 0.00005 | 0.00000 | 0.00000 | 0.00000 | 0.00935 |
| 6 | Sep. 05, 2003 | 73800 | 0.6 | 0.01696 | 0.00623 | 0.00333 | 0.00178 | 0.00108 | 0.00144 | 0.00058 | 0.00020 | 0.00009 | 0.00008 | 0.00007 | 0.00001 | 0.03187 |
| 7 | Sep. 05, 2003 | 68869 | 0.6 | 0.01340 | 0.00623 | 0.00370 | 0.00197 | 0.00129 | 0.00123 | 0.00070 | 0.00022 | 0.00010 | 0.00010 | 0.00003 | 0.00001 | 0.02900 |
| 8 | Sep. 06, 2003 | 27437 | 0.6 | 0.00303 | 0.00284 | 0.00303 | 0.00124 | 0.00138 | 0.00109 | 0.00047 | 0.00015 | 0.00018 | 0.00007 | 0.00011 | 0.00000 | 0.01359 |
| 9 | Sep. 06, 2003 | 16060 | 0.5 | 0.01494 | 0.01283 | 0.00878 | 0.00380 | 0.00218 | 0.00386 | 0.00374 | 0.00125 | 0.00031 | 0.00050 | 0.00050 | 0.00000 | 0.05268 |
| 10 | Sep. 06, 2003 | 8550 | 0.6 | 0.05170 | 0.03977 | 0.02456 | 0.00842 | 0.00632 | 0.01099 | 0.00971 | 0.00281 | 0.00211 | 0.00257 | 0.00152 | 0.00023 | 0.16070 |
| 11 | Mar. 27, 2005 | 32278 | 0.5 | 0.30910 | 0.13830 | 0.05134 | 0.01230 | 0.00403 | 0.00437 | 0.00251 | 0.00127 | 0.00056 | 0.00084 | 0.00056 | 0.00003 | 0.52519 |
| 12 | Feb. 22, 2006 | 20592 | 0.45 | 0.01520 | 0.01705 | 0.01151 | 0.00490 | 0.00189 | 0.00199 | 0.00078 | 0.00024 | 0.00010 | 0.00015 | 0.00000 | 0.00000 | 0.05381 |
| 13 | Jan. 15, 2007 | 89133 | 0.45 | 0.13087 | 0.05092 | 0.00928 | 0.00468 | 0.00220 | 0.00223 | 0.00112 | 0.00040 | 0.00016 | 0.00010 | 0.00004 | 0.00000 | 0.20201 |
| 14 | Jan. 27, 2007 | 23474 | 0.3 | 0.14633 | 0.10075 | 0.05725 | 0.02151 | 0.00750 | 0.00660 | 0.00379 | 0.00158 | 0.00072 | 0.00098 | 0.00038 | 0.00021 | 0.34762 |
| 15 | Mar. 28, 2007 | 77851 | 0.4 | 0.03857 | 0.01992 | 0.01879 | 0.01281 | 0.00518 | 0.00369 | 0.00089 | 0.00013 | 0.00005 | 0.00003 | 0.00000 | 0.00000 | 0.10005 |
| 16 | Apr. 06, 2007 | 32852 | 0.55 | 0.03930 | 0.02052 | 0.00682 | 0.00161 | 0.00091 | 0.00119 | 0.00094 | 0.00027 | 0.00015 | 0.00015 | 0.00018 | 0.00000 | 0.07205 |

B

| Image metadata | | | | Size-specific mass ($10^{12}$ kg km$^{-2}$) | | | | | | | | | | | | |
|---|---|---|---|---|---|---|---|---|---|---|---|---|---|---|---|---|
| | | | | Size classes (area in km$^2$) | | | | | | | | | | | | Total |
| Image | Date | Area (km$^2$) | Threshold | 0.005 | 0.01 | 0.025 | 0.05 | 0.075 | 0.1 | 0.2 | 0.3 | 0.4 | 0.5 | 1 | 2 | Mass |
| 1 | Dec. 28, 1996 | 9149 | 0.5 | 0.00097 | 0.00199 | 0.00430 | 0.00634 | 0.00478 | 0.00713 | 0.00696 | 0.00383 | 0.00267 | 0.00333 | 0.00121 | 0.00181 | 0.04532 |
| 2 | Jan. 21, 1997 | 14822 | 0.7 | 0.00260 | 0.00208 | 0.00269 | 0.00311 | 0.00283 | 0.00407 | 0.00345 | 0.00150 | 0.00082 | 0.00103 | 0.00075 | 0.00037 | 0.02530 |
| 3 | Mar. 10, 1997 | 28460 | 0.7 | 0.00036 | 0.00068 | 0.00100 | 0.00070 | 0.00031 | 0.00029 | 0.00009 | 0.00002 | 0.00004 | 0.00015 | 0.00019 | 0.00000 | 0.00383 |
| 4 | Jan. 20, 1998 | 20481 | 0.5 | 0.00002 | 0.00008 | 0.00019 | 0.00021 | 0.00012 | 0.00011 | 0.00000 | 0.00000 | 0.00005 | 0.00000 | 0.00000 | 0.00000 | 0.00079 |
| 5 | Jan. 20, 1998 | 19153 | 0.5 | 0.00002 | 0.00005 | 0.00020 | 0.00014 | 0.00009 | 0.00008 | 0.00000 | 0.00000 | 0.00006 | 0.00000 | 0.00000 | 0.00000 | 0.00063 |
| 6 | Sep. 05, 2003 | 73800 | 0.6 | 0.00019 | 0.00014 | 0.00019 | 0.00020 | 0.00018 | 0.00032 | 0.00026 | 0.00014 | 0.00011 | 0.00011 | 0.00019 | 0.00007 | 0.00210 |
| 7 | Sep. 05, 2003 | 68869 | 0.6 | 0.00015 | 0.00014 | 0.00021 | 0.00022 | 0.00022 | 0.00028 | 0.00031 | 0.00015 | 0.00011 | 0.00014 | 0.00008 | 0.00008 | 0.00209 |
| 8 | Sep. 06, 2003 | 27437 | 0.6 | 0.00003 | 0.00006 | 0.00017 | 0.00014 | 0.00023 | 0.00024 | 0.00021 | 0.00010 | 0.00020 | 0.00010 | 0.00030 | 0.00000 | 0.00180 |
| 9 | Sep. 06, 2003 | 16060 | 0.5 | 0.00017 | 0.00029 | 0.00049 | 0.00042 | 0.00037 | 0.00087 | 0.00167 | 0.00083 | 0.00034 | 0.00069 | 0.00138 | 0.00000 | 0.00753 |
| 10 | Sep. 06, 2003 | 8550 | 0.6 | 0.00058 | 0.00089 | 0.00138 | 0.00095 | 0.00106 | 0.00247 | 0.00435 | 0.00188 | 0.00234 | 0.00357 | 0.00422 | 0.00130 | 0.02499 |
| 11 | Mar. 27, 2005 | 32278 | 0.5 | 0.00346 | 0.00310 | 0.00288 | 0.00138 | 0.00068 | 0.00098 | 0.00112 | 0.00086 | 0.00062 | 0.00116 | 0.00155 | 0.00017 | 0.01795 |
| 12 | Feb. 22, 2006 | 20592 | 0.45 | 0.00017 | 0.00038 | 0.00065 | 0.00055 | 0.00032 | 0.00045 | 0.00035 | 0.00017 | 0.00011 | 0.00020 | 0.00000 | 0.00000 | 0.00334 |
| 13 | Jan. 15, 2007 | 89133 | 0.45 | 0.00147 | 0.00114 | 0.00052 | 0.00052 | 0.00037 | 0.00050 | 0.00050 | 0.00027 | 0.00017 | 0.00014 | 0.00012 | 0.00000 | 0.00573 |
| 14 | Jan. 27, 2007 | 23474 | 0.3 | 0.00164 | 0.00226 | 0.00321 | 0.00241 | 0.00126 | 0.00148 | 0.00170 | 0.00106 | 0.00081 | 0.00136 | 0.00107 | 0.00118 | 0.01943 |
| 15 | Mar. 28, 2007 | 77851 | 0.4 | 0.00043 | 0.00045 | 0.00105 | 0.00143 | 0.00087 | 0.00083 | 0.00040 | 0.00009 | 0.00006 | 0.00004 | 0.00000 | 0.00000 | 0.00564 |
| 16 | Apr. 06, 2007 | 32852 | 0.55 | 0.00044 | 0.00046 | 0.00038 | 0.00018 | 0.00015 | 0.00026 | 0.00042 | 0.00019 | 0.00017 | 0.00021 | 0.00051 | 0.00000 | 0.00337 |

| Iceberg | Elevation (m) | Area ($10^6$ $m^2$) | Subaerial volume ($10^6$ $m^3$) | Total mass ($10^{12}$ kg) |
|---|---|---|---|---|
| A5201 | 25.3 +/- 5.8 | 300.8 | 7610.2 | 51.8 |
| A5202 | 32.5 +/- 4.4 | 30.81 | 1001.3 | 6.8 |
| W86 | 41.2 +/- 3.5 | 0.125 | 5.15 | 0.035 |
| W87 | 51.0 +/- 7.0 | 0.463 | 23.61 | 0.16 |

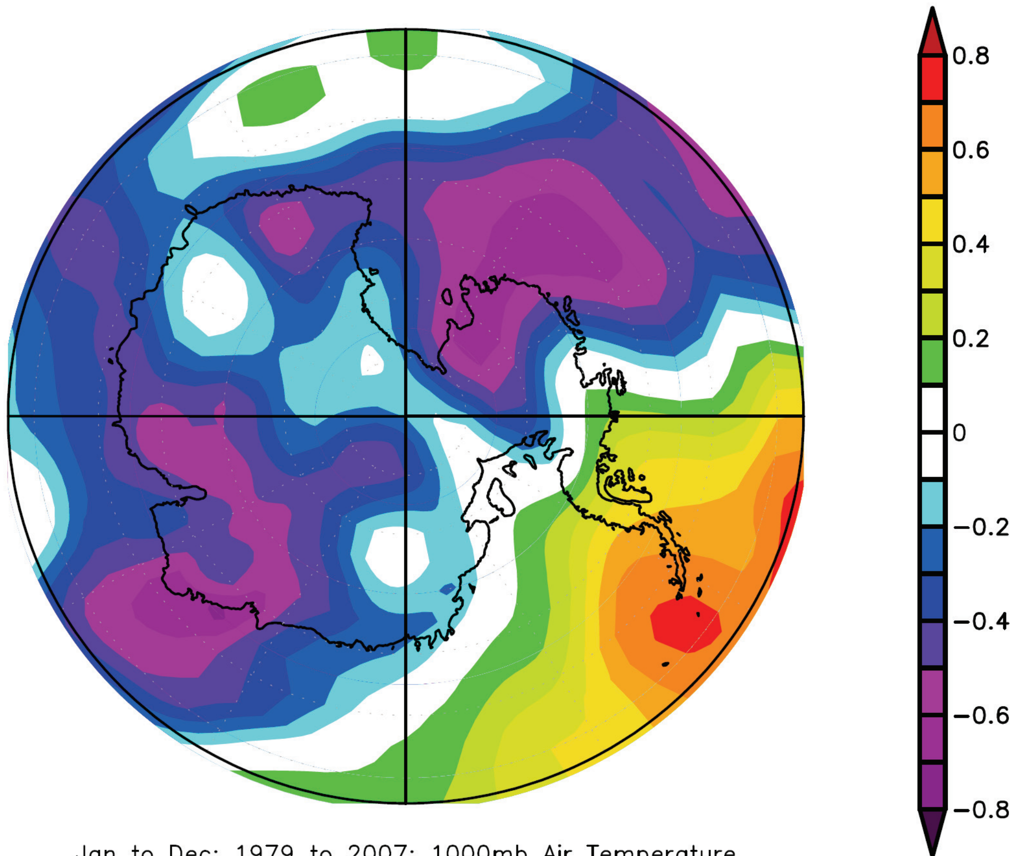


Jan to Dec: 1979 to 2007: 1000mb Air Temperature
Seasonal Correlation w/ Jan to Dec AAO

NCEP/NCAR Reanalysis

NOAA/ESRL Physical Sciences Division

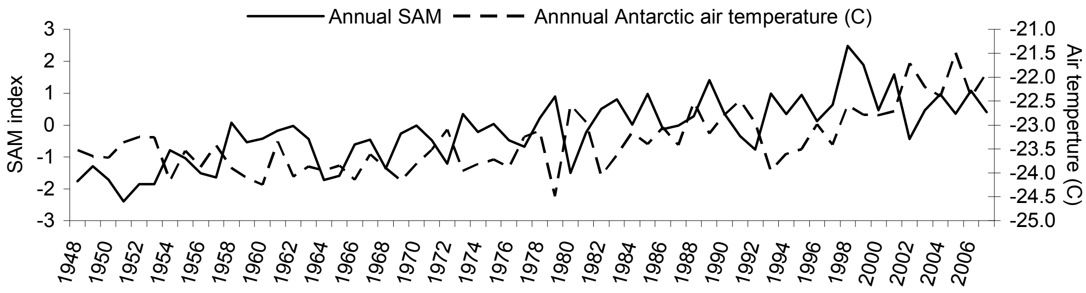
Annual SAM
Annnual Antarctic air temperature (C)
SAM index
Air temperture (C)
3
2
1
0
-1
-2
-3
-21.0
-21.5
-22.0
-22.5
-23.0
-23.5
-24.0
-24.5
-25.0
1948
1950
1952
1954
1956
1958
1960
1962
1964
1966
1968
1970
1972
1974
1976
1978
1980
1982
1984
1986
1988
1990
1992
1994
1996
1998
2000
2002
2004
2006